A velocity transformation for rough-wall-bounded turbulent flows

By B. Bornhoft, S. S. Jain and P. Moin

1. Motivation and objectives

Rough-wall turbulent flows are ubiquitous in fluid mechanics. Several critical components in various propulsion and turbomachinery devices are subject to conditions in which the flow within the boundary layers interacts with surface roughness. For instance, wind turbines and aircraft lifting surfaces experience leading-edge ice accretion, compressor blades suffer from erosive damage, turbine blades are roughened by molten particulate deposition and limited precision in additive manufacturing/3D printing engender small-scale roughness. In all of these instances, the aerodynamic performance and operability are compromised by the presence of surface roughness.

The primary impact of various types of roughness on wall-bounded turbulent flows is the downward shift of the mean velocity profile (in semilogarithmic plots), which indicates an increase in drag. This can be modeled by incorporating the offset in the mean velocity, known as the roughness function, ΔU^+ (Clauser 1954; Hama 1954). Hama (1954) proposed the roughness function as a function of the equivalent sand-grain roughness height, k_s^+, where

$$\Delta U^+(k_s^+) = \frac{1}{\kappa}\ln(k_s^+) + B - B_r(k_s^+). \tag{1.1}$$

Here, $B = 5.2$ represents the log-law intercept for a smooth wall, and $B_r(\infty) = 8.5$ denotes the modification to the log intercept in the fully-rough regime. The equivalent sand-grain roughness height is a hydrodynamic quantity that represents "the grain size of uniform (monodisperse), close-packed sand grains on a hypothetical surface that would cause the same drag as the surface of interest if exposed to the same flow in the fully rough regime" (Chung *et al.* 2021). It is important to note that Eq. (1.1) is applicable only to the fully-rough regime ($k_s^+ \gtrsim 80$) and necessitates knowledge of the underlying flow field, being defined in terms of hydrodynamic variables (Kadivar *et al.* 2021). For situations in the transitional rough regime, other proposed roughness functions provide modifications. For instance, functions aligned with the traditional Nikuradse experiments (Nikuradse 1932) can be expressed as (Demirel *et al.* 2017)

$$\Delta U^+(k_s^+) = \begin{cases} 0 & \text{if} \quad k_s^+ < 3 \\ \frac{1}{\kappa}\ln(0.26k_s^+) \times \sin\left(\frac{\pi}{2}\frac{\ln(k_s^+/3)}{\ln(5)}\right) & \text{if} \quad 3 < k_s^+ < 15 \\ \frac{1}{\kappa}\ln(0.26k_s^+) & \text{if} \quad k_s^+ > 15. \end{cases} \tag{1.2}$$

Other approaches, such as those fitting experimental data from Colebrook & White (1937) and Colebrook *et al.* (1939), can be expressed as (Grigson 1987)

$$\Delta U^+(k_s^+) = \frac{1}{\kappa}\ln\left(1 + \frac{k_s^+}{e^{3.25\kappa}}\right). \tag{1.3}$$

In all these fits, either k_s^+ or ΔU^+ requires additional modeling to predict the impact of a rough surface on the boundary layer. In this study, we directly model the roughness function, ΔU^+, as it is conducive to modifying wall models for large-eddy simulations.

In addition to the shift in the log law, there are other modifications to the mean velocity profile in the viscous sublayer; for rough surfaces, we call this region the roughness sublayer (RSL). These additional modifications to the mean velocity profile include: (i) the change of slope (a_c, see Figure 1) in the RSL compared to the viscous sublayer in smooth-wall turbulent boundary layers, where the slope is unity; (ii) the mean velocity at $y^+ = 0$ near the wall ($U^+(0) \neq 0$, see Figure 1), which is otherwise zero for a smooth wall; and (iii) the extent of the RSL and where it transitions to the log-layer behavior. In Figure 1(a), we highlight an example of a turbulent boundary layer velocity profile for both a clean and rough surface at $Re_\tau = 180$ plotted in inner units, for example, $U^+ = U/u_\tau$ and $y^+ = yu_\tau/\nu$, where the spatially averaged friction velocity is defined as $u_\tau = \sqrt{\tau_w/\rho}$, with τ_w as the wall shear stress, ρ the fluid density and y^+ the coordinate normal to the plane of the arithmetic mean roughness height. These are representative direct numerical simulations (DNSs) from the work of Thakkar *et al.* (2017). The two inset figures of Figure 1(a) illustrate the described modifications in the RSL.

Rough surfaces can be characterized using various parameters, such as the average roughness height (k_a), root-mean-square (RMS) roughness height (k_{rms}), effective slope (ES), solidity (Λ), skewness (s_k) and their spacing. Detailed definitions of these parameters can be found in Jimenez (2004), Kadivar *et al.* (2021) and Chung *et al.* (2021). It has been shown that roughness requires at least two or more parameters to appropriately characterize its effect on near-wall turbulent flows (De Marchis *et al.* 2020; Kadivar *et al.* 2021; Flack & Chung 2022). Various correlations have been proposed to model roughness elements in different flow configurations (Forooghi *et al.* 2017; Kuwata & Kawaguchi 2019; De Marchis *et al.* 2020; Flack *et al.* 2020; Jouybari *et al.* 2021; Ma *et al.* 2023; Yang *et al.* 2023). However, the search for a universal roughness model is still an active area of research. A significant challenge in using the available correlations in the literature to develop a roughness subgrid model is the reliance of the correlations on the effective hydrodynamic roughness length scale instead of a geometric roughness length scale, which limits the predictive capability of such correlations.

In this work, we gather a roughness database from available DNS datasets to construct a velocity transformation for rough-wall-bounded turbulent channel flows. We divide the mean velocity profiles into two regions: the RSL and the log layer. Within each region, we construct correlations that incorporate at least two roughness parameters for (i) the log-layer roughness function, (ii) the slope of the RSL (a_c) and (iii) the averaged velocity at the arithmetic mean location of the rough surface [$\Delta U^+_{RSL} \equiv U^+(y^+ = 0)$]. For ΔU^+, we compare the correlation that we developed to the existing correlations in the literature. To the best of our knowledge, this is the first parameterization of the RSL with respect to geometric features. A velocity transformation that uses these correlations is then evaluated using available DNS velocity profiles.

2. Construction of a DNS database

A DNS database containing turbulent rough-wall channel flows is constructed to study how various roughness parameters influence mean flow properties. Mean velocity profiles and roughness statistics are extracted from available DNS data in the literature. A total of 98 rough-wall channel and pipe flows spanning both the transitional ($k_s^+ < 80$) and

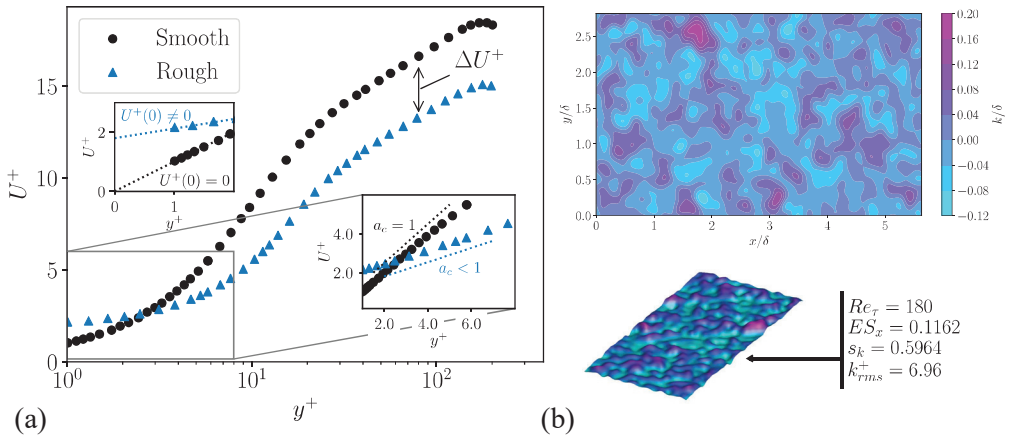

FIGURE 1. (a) Schematic highlighting the changes occurring in a smooth-wall boundary layer when bounded by a rough wall. Specific attention is paid to highlighting the modeling parameters of ΔU^+, a_c and $U^+(0)$. An example smooth-channel DNS result of Thakkar *et al.* (2017) at $Re_\tau = 180$ is included as a reference in (a). (b) Examples of specific roughness geometry values (Thakkar *et al.* 2017).

Paper	Number of cases	Symbol	Re_τ	k_a^+	k_{rms}^+	ES	s_k
Chan *et al.* (2015)	14	▲	180–540	1.01–32.4	1.25–40	0.09–0.361	0
Chan *et al.* (2018)	4	●	540	24	30	0.27–0.72	0
Thakkar *et al.* (2017)	16	✚	180	4.37–7.42	5.7–9.17	0.06–0.32	–0.52–0.6
Thakkar *et al.* (2018)	8	■	180–720	0.62–19.8	0.8–25.75	0.23	–0.52
Ma *et al.* (2021)	2	◀	400–600	2.22	2.78	0.265	–0.053
Busse & Jelly (2023)	7	✖	395	6.636–10.3885	9.243–13.035	0.198–0.209	–2.3–2.3
Jouybari *et al.* (2021)	32	▶	1000	6.6–36.7	8.2–43.7	0.07–0.92	–0.22–2.37
Total	83		180–1000	0.62–36.7	0.8–43.7	0.06–0.92	–2.3–2.37

TABLE 1. Details of the constructed DNS database.

fully-rough ($k_s^+ > 80$) regimes are considered with various roughness topographies. Of these geometries, we utilize 83 to develop our model. The geometries excluded fall into one of three categories: (i) highly dense roughness where the predominant length scale becomes a gap-based Reynolds number, found in canopy-type roughness (here, we define these surfaces as $ES \geq 0.5$ and $s_k \leq -0.1$); (ii) surfaces with highly non-isotropic slopes, whose ratio of slopes (in the streamwise and spanwise directions) exceed 10; and (iii) geometries well within the wavy regime ($\lambda^+ > 800$). These surfaces require additional modeling, specifically in the roughness buffer layer. Table 1 includes details of the various cases. In particular, we focus on the variations in the *RMS* height, k_{rms}^+, the streamwise ES, and the skewness, s_k, as critical parameters for our investigation. The variation in topography across the different rough surfaces results in a broad spectrum of velocity profiles. In Figure 2(a), velocity profiles normalized by inner units are plotted on a semi-log scale. Each profile can be unique and varies drastically between the surfaces. Using a velocity transformation based on the developed correlations, we find a reasonable collapse amongst this wide variation in velocity profiles.

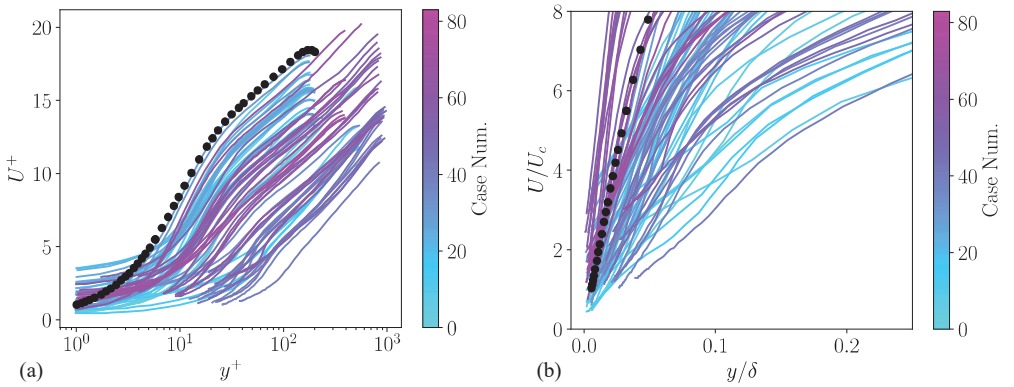

FIGURE 2. Extracted DNS rough-wall boundary layer profiles from the database in Table 1 plotted in (a) inner and (b) outer units. For reference, an example smooth channel DNS result from Thakkar *et al.* (2017) at $Re_\tau = 180$, denoted by ●, is included. The case number corresponds to the order in Table 1, increasing from the top to the bottom of the table.

3. Constant stress layer assumption in roughness sublayer

In Figure 2(b), velocity profiles in the near-wall region are plotted in outer units. We observe that in the near-wall region, the rough-wall velocities largely behave linearly. This observation has also been made in the rough-bed flow literature. Nikora *et al.* (2004) postulated three RSL models based on (i) a constant velocity profile, (ii) an exponential profile and (iii) a linear profile. Each of these was tested against a data set of experimental rough-bed flows, and it was found that both the exponential and linear profiles were acceptable. In our rough-wall channel data set, we primarily observe a linear behavior. Therefore, we represent the RSL with a linear profile. To accomplish this, we consider the space-time-averaged shear stress, where $\langle \tau_w \rangle$ represents the spatial average in the (x, z) plane, and $\overline{\tau_w}$ is the temporal average for a rough surface

$$\langle \overline{\tau(y)} \rangle = \nu_R \frac{d\langle \overline{U} \rangle}{dy}. \tag{3.1}$$

Here, ν_R is an effective roughness viscosity value explicitly dependent upon the form-induced stresses and form drag of the rough wall [$\nu_R = f(f_p, f_v)$] (Nikora *et al.* 2001). Given our linear profile assumption within the RSL, we postulate that within the RSL, we have a constant stress layer leading to

$$\frac{\langle \overline{U(y)} \rangle}{u_\tau} = \frac{u_\tau y}{\nu_R} + \frac{\langle \overline{U(0)} \rangle}{u_\tau}. \tag{3.2}$$

Here, the model adjusts the viscosity within the RSL given a particular roughness topography where $\nu_R = (1/a_c)\nu$. Using the constant shear stress assumption, we recover

$$U^+_{RSL} = a_c y^+ + \Delta U^+_{RSL}. \tag{3.3}$$

In Eq. (3.3), $a_c \approx f(k_a^+, k_{rms}^+, ES, s_k, ...)$ represents the change in slope of the velocity near the rough wall, and $\Delta U^+_{RSL} \approx f(k_a^+, k_{rms}^+, ES, s_k, ...)$ represents the averaged velocity observed at the arithmetic mean of the rough surface. Outside of the RSL, we model the logarithmic layer by the classical law of the wall shifted by a roughness function,

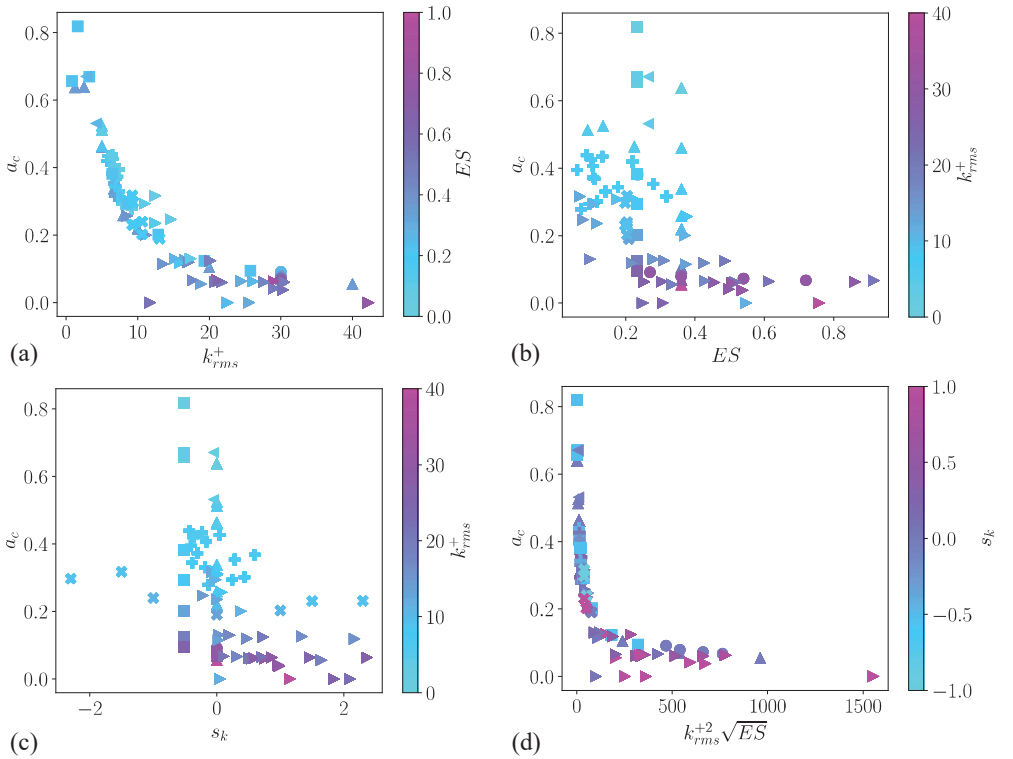

FIGURE 3. Dependence of the inverse roughness viscosity, a_c, on geometrical parameters: (a) k^+_{rms}, (b) ES, (c) s_k and (d) $k^{+2}_{rms}\sqrt{ES}$. Mappings of symbols to relevant studies can be found in Table 1.

$\Delta U^+ \approx f(k^+_a, k^+_{rms}, ES, s_k, ...)$, where

$$U^+ = \frac{1}{\kappa}\ln y^+ + B - \Delta U^+. \tag{3.4}$$

To ensure a continuous velocity profile, we enforce C^0 continuity between Eqs. (3.3) and (3.4). Sections 4 to 6 address correlations of these terms and propose fits accordingly.

4. Roughness viscosity correlation

Understanding the behavior of the inverse of roughness viscosity, a key representation of the change in slope in the RSL, is crucial for modeling the turbulent velocity profile. In this section, we investigate how a_c correlates with three important parameters: k^+_{rms}, ES and s_k. In Figure 3, the relationship between a_c and these parameters, as well as their combinations, is illustrated. Figure 3(a) highlights a strong correlation between k^+_{rms} and a_c. As the inner-scaled roughness height increases, the slope of the RSL decreases. A similar trend is observed with increasing ES in Figure 3(b). While s_k shows a weaker correlation, the higher skewness values appear to correspond to a smaller slope. However, this correlation might be influenced by the increased k^+_{rms} for cases with high skew.

Figure 3(d) presents the slope of the RSL for a combination of k^+_{rms} and ES. A reasonable collapse is observed where the best fit is achieved when using $k^2_{rms}\sqrt{ES}$. The function behaves logarithmically if we consider the inverse of the independent variable.

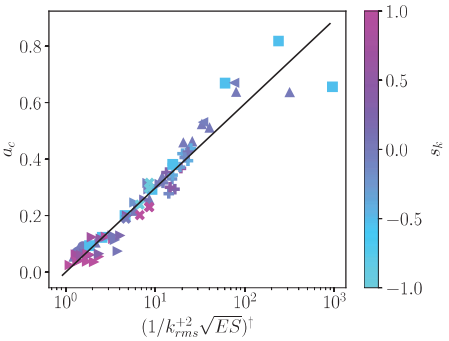

FIGURE 4. Dependence of a_c with respect to $(1/(k_{rms}^{+2}\sqrt{ES}))^\dagger$, where $x^\dagger = c_2 x + c_3$.

Based on this observation, we propose the following functional form for the a_c model

$$a_c = c_1 \ln(c_2 x + c_3), \tag{4.1}$$

where c_1, c_2 and c_3 are fitting constants. The final proposed model and fitting function are plotted in Figure 4, where $x^\dagger = c_2 x + c_3$ and $x = 1/(k_{rms}^2\sqrt{ES})$. This approach achieves an $r^2 = 90.3\%$ fit, where

$$r^2 = 1 - \left(\frac{\sum (a_{c,DNS} - a_c)^2}{\sum (a_{c,DNS} - \overline{a_c})^2} \right). \tag{4.2}$$

Busse & Jelly (2023) found that the roughness function was related to s_k by a weighted hyperbolic tangent function. Following the work of Busse & Jelly (2023), we modify Eq. (4.1) to include asymmetries introduced by s_k. The new proposed fit

$$a_c = c_1 \ln(c_2 x + c_3)[(c_4 - 1)\tanh(c_5 s_k) + 1] \tag{4.3}$$

improves the fit to 93.3%, which is acceptable given the wide variety of roughness topologies considered.

5. Mean roughness velocity intercept correlation

Following a methodology similar to that in Section 4, we investigate correlations between roughness parameters and the mean roughness velocity intercept, ΔU^+_{RSL}. In Figure 5(a), a weak correlation is observed between ΔU^+_{RSL} and k^+_{rms}, where in general, ΔU^+_{RSL} increases with increasing k^+_{rms}. This can be observed by looking at individual symbol groups, such as those by Thakkar *et al.* (2017) [✚, in Figure 5(a)] or Chan *et al.* (2015) [▲, in Figure 5(a)], where increased roughness heights result in increased ΔU^+_{RSL}. Figure 5(b) reveals an inverse relationship between ES and ΔU^+_{RSL}, where increased slopes result in near-zero velocity at the arithmetic mean roughness height. Additionally, symbols colored by k^+_{rms} increase in value from the bottom left to the top right of Figure 5(b). This shows a direct relation between the roughness height and effective slope for the velocity at the arithmetic mean geometric location. Little correlation with skewness is observed in Figure 5(c). Therefore, we postulate that k^+_{rms} and ES are the critical parameters influencing the mean roughness velocity intercept correlation. In Figure 5(d), we explore the relationship between k^+_{rms} and ES as a ratio, considering it as a model for the average wavelength of the roughness topology. Weighting the effective slope in

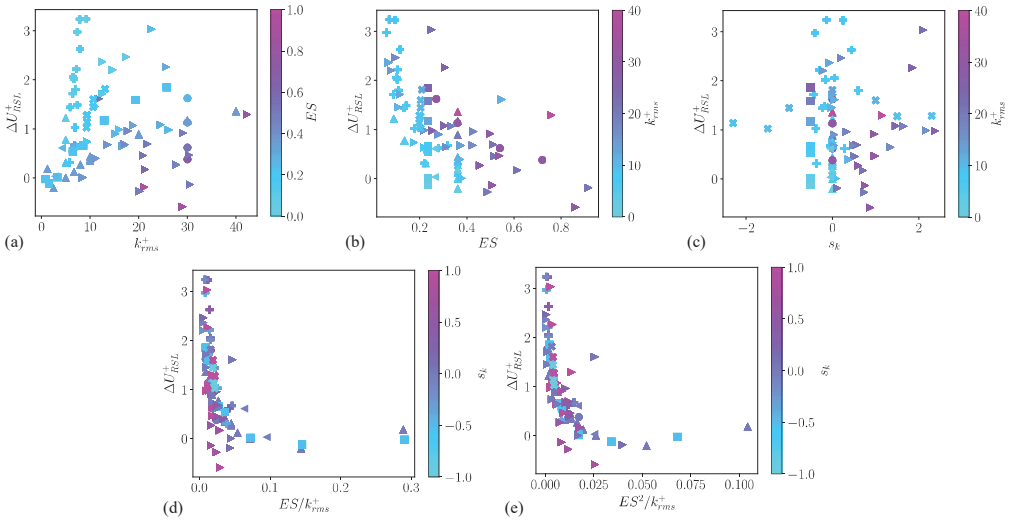

FIGURE 5. Dependence of ΔU^+_{RSL} on geometrical parameters: (a) k^+_{rms}, (b) ES, (c) s_k, (d) ES/k^+_{rms} and (e) ES^2/k^+_{rms}. Mappings of symbols to relevant studies can be found in Table 1.

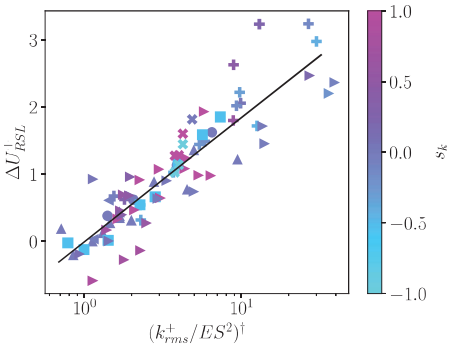

FIGURE 6. Dependence of ΔU^+_{RSL} with respect to $(k^+_{rms}/ES^2)^\dagger$, where $x^\dagger = c_2 x + c_3$.

Figure 5(e) improves the best-fit correlation. Utilizing the same model form as Eq. (4.1), we propose the following expression for the ΔU^+_{RSL} model

$$\Delta U^+_{RSL} = c_1 \ln(c_2 x + c_3), \tag{5.1}$$

where $x = k^+_{rms}/ES^2$. This model results in a 81.0% fit, as depicted in Figure 6. While the overall fit may not be as accurate as the roughness viscosity correlation, this intercept introduces less absolute error to the total velocity fit.

6. Roughness function correlation

Correlations for the roughness function, ΔU^+, or the equivalent sand-grain roughness, k^+_s, have been proposed by numerous research groups (Forooghi *et al.* 2017; Kuwata & Kawaguchi 2019; Flack *et al.* 2020; Jouybari *et al.* 2021; Ma *et al.* 2023; Yang *et al.* 2023). Each correlation is based on the data available to the authors, making the model's performance contingent upon the specific roughness characteristics considered. Previous

studies have developed their models by incorporating one, two, three or more roughness parameters. Recent work by Flack & Chung (2022) consolidated these various approaches into a comprehensive table. Chung *et al.* (2021) postulated that a predictive roughness function should incorporate at least three parameters: (i) the roughness height, (ii) a description of the frontal area and (iii) a description of the surface coverage. Here, we leverage the DNS database to develop a three-parameter model, incorporating k^+_{rms}, ES and s_k, with improved performance compared to existing two-parameter models (Chan *et al.* 2015; De Marchis *et al.* 2020; Flack *et al.* 2020).

Figure 7 illustrates the behaviors of the roughness function concerning various roughness parameters and their combinations. A strong dependence of the roughness function on k^+_{rms} is evident in Figure 7(a). In Figure 7(b), we observe a similar trend to that of Napoli *et al.* (2008), where at high ES we begin to observe a plateau in ΔU^+, and as ES goes to zero we observe a quick decay in the roughness function. Skewness exhibits a noticeable impact in specific studies, such as in Busse & Jelly (2023) [✖ values in Figure 7(c)], where they fixed the roughness height and slope while varying the skewness parameter and observed that the roughness function behaved similarly to an asymmetric hyperbolic tangent function. Building on the insights of De Marchis *et al.* (2020), we plot ΔU^+ with respect to $k^+_{rms}ES$. Similar to their results, a strong logarithmic correlation is observed. Flack *et al.* (2020) determined that additional considerations are likely necessary for surfaces approaching the wavy regime.

We explore an exponential response of ES for the roughness function in Figure 7(e) and find a notable correlation between the variables. Combining the ideas from Figure 7(d,e) in Figure 7(f) yields reasonable collapse among the data.

We adopt the model form of Eq. (4.1) with three coefficients and set $x = k^+_{rms}ES$. In refining this model, we draw insights from Figure 7(c,e). Adjusting the model to accommodate skewness and account for surfaces with higher ES prompts us to propose the following modified model form for the roughness function

$$\Delta U^+ = c_1 \ln\left(c_2 k^+_{rms} ES\right)\left[(c_3 - 1)\tanh\left(c_4 s_k\right) + 1\right] e^{-c_5 ES^{c_6}}. \tag{6.1}$$

This final form of the roughness function yields a 95.4% fit with the available DNS database. Table 2 compares two-parameter models available in the literature by Flack *et al.* (2020), Kuwata & Kawaguchi (2019), Chan *et al.* (2015) and De Marchis *et al.* (2020). The proposed models of Flack *et al.* (2020) and Kuwata & Kawaguchi (2019) directly compute k^+_s as a function of k^+_{rms} and s_k. Therefore, to compare these fits to those directly finding correlations for the roughness function ΔU^+, we must apply a roughness function. We use three roughness functions widely accepted in the literature to compute ΔU^+ given the modeled k^+_s: Hama type [Hama (1954), Eq. (1.1)], Nikuradse type [Demirel *et al.* (2017), Eq. (1.2)], and Colebrook type [Colebrook & White (1937), Eq. (1.3)]. Across all correlations, we find that the proposed model best fits the current DNS database.

7. Transformation of rough-wall turbulent channel flows

Utilizing the correlations for the three parameters, we develop a transformation to collapse rough-wall boundary layers to the classical smooth-wall boundary layer. In the smooth wall viscous sublayer, $U^+ = y^+$. Equation 3.3 is solved for y^+ and scaled by $y^{\dagger,s}/y^\dagger$, where $y^{\dagger,s}$ is the wall-normal location of C^0 continuity at the transition location between the viscous sublayer and log layer for the smooth-wall, and $y^\dagger$ is the C^0 location

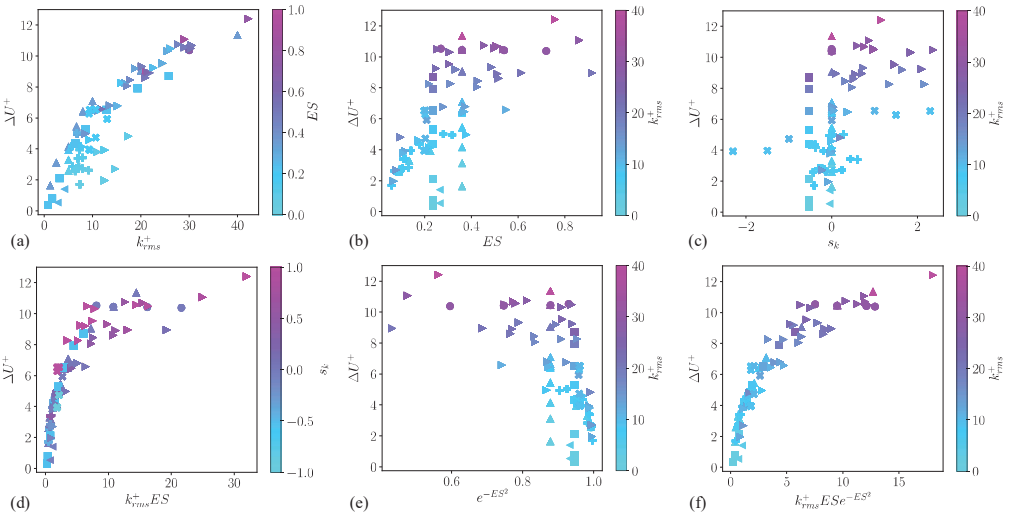

FIGURE 7. Dependence of the roughness function, ΔU^+, on geometrical parameters: (a) k^+_{rms}, (b) ES, (c) s_k, (d) $k^+_{rms}ES$, (e) e^{-ES^2} and (f) $k^+_{rms}ES e^{-ES^2}$. Mappings of symbols to relevant studies can be found in Table 1.

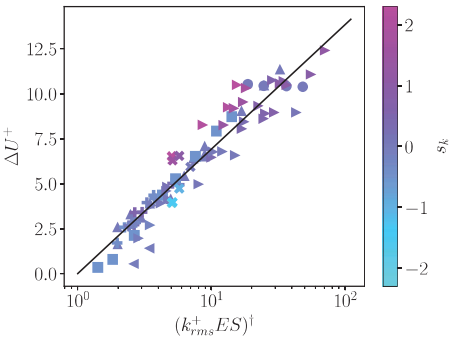

FIGURE 8. Dependence of ΔU^+ with respect to $(k_{rms}ES)^\dagger$, where $x^\dagger = c_2 x$.

between the surface's RSL and log layer. We define this value as U^*_{RSL}, where

$$U^*_{\mathrm{RSL}} = \left(\frac{U^+ - \Delta U^+_{RSL}}{a_c} \right) \frac{y^{\dagger,s}}{y^\dagger}. \tag{7.1}$$

The corresponding wall-normal coordinate is then shifted by the difference in continuity locations between the smooth and rough walls, given by

$$y^* = y^+ + (y^{\dagger,s} - y^\dagger). \tag{7.2}$$

The log layer is shifted by the rough surface's roughness function ($U^*_{\log} = U^+ + \Delta U^+$), recovering the classical law of the wall function. In Figure 9, we present (a) all of the DNS data in inner units, (b) the transformed DNS data with the transformations defined in Eqs. (7.1) and (7.2) and (c) the transformed data using the model fits from Eqs. (4.3), (5.1) and (6.1) with the coefficient values detailed in Table 3. We observe a good collapse to the smooth-wall data when directly applying the DNS data to the model form in Figure 9(b). Although the spread increases when applying the modeled values of ΔU^+, a_c and

Correlation	Model Form	Roughness Function	r^2
Flack *et al.* (2020)	$k_s^+ = \begin{cases} 2.73k_{rms}^+ (2+s_k)^{-0.45} & \text{if} \quad s_k < 0.0 \\ 2.11k_{rms}^+ & \text{if} \quad s_k = 0.0 \\ 2.48k_{rms}^+ (1+s_k)^{2.24} & \text{if} \quad s_k > 0.0 \end{cases}$	Eq. (1.1) Eq. (1.2) Eq. (1.3)	0.540 0.536 0.619
Kuwata & Kawaguchi (2019)	$k_s^+ = \begin{cases} 4.0k_{rms}^+ (1+0.17s_k)^4 & \\ 2.48k_{rms}^+ (1+s_k)^{2.24} & \text{if} \quad s_k > 0.0 \end{cases}$	Eq. (1.1) Eq. (1.2) Eq. (1.3)	0.670 0.666 0.669
Chan *et al.* (2015)	$\Delta U^+ = \frac{1}{\kappa} \log\left(k_a^+\right) + 1.12ES + 1.47$	N/A	0.650
De Marchis *et al.* (2020)	$\frac{1}{\kappa} \log\left(ESk_{rms}^+\right) + 3.5$	N/A	0.917
Proposed model	See Eq. (6.1)	N/A	0.954

TABLE 2. Comparison of the best-fit performance of selected roughness functions from the literature.

Term	Coeff.	Value	Term	Coeff.	Value	Term	Coeff.	Value
ΔU^+	c_1	3.026	a_c	c_1	0.123	ΔU_{RSL}^+	c_1	0.799
	c_2	3.444		c_2	318.15		c_2	0.0143
	c_3	28.56		c_3	1.124		c_3	0.574
	c_4	0.0031		c_4	0.144			
	c_5	0.353		c_5	0.114			
	c_6	0.894						

TABLE 3. Fitting coefficients for the model functions.

ΔU_{RSL}^+, a general collapse to the smooth-wall boundary layer profile is still apparent. Given the limited roughness statistics applied (k_{rms}^+, ES and s_k), we consider this an acceptable fit.

8. Conclusions

In this study, we present a novel velocity transformation for turbulent flows over rough walls, leveraging a concise set of rough-wall geometric parameters: k_{rms}^+, ES and s_k. We construct a DNS database to characterize the modification to the classical smooth-wall boundary layer. In the RSL, we adopt a constant shear stress approximation motivated by the observed linearity in most roughness sublayers. This model, coupled with the log-layer shift, enables the parameterization of the rough-wall boundary layer profile using three key terms: the log-layer shift or roughness function, ΔU^+, the change in slope of the near-wall RSL, a_c, and the change in the velocity at the arithmetic mean of the rough surface, ΔU_{RSL}^+. We parameterize each of these terms using a minimal set of roughness statistics. Correlations between the variables are identified and used to construct model functions to fit the available data. Comparisons between the spread in the DNS data, the model form, and the modeled transformation demonstrate a reasonable collapse across all

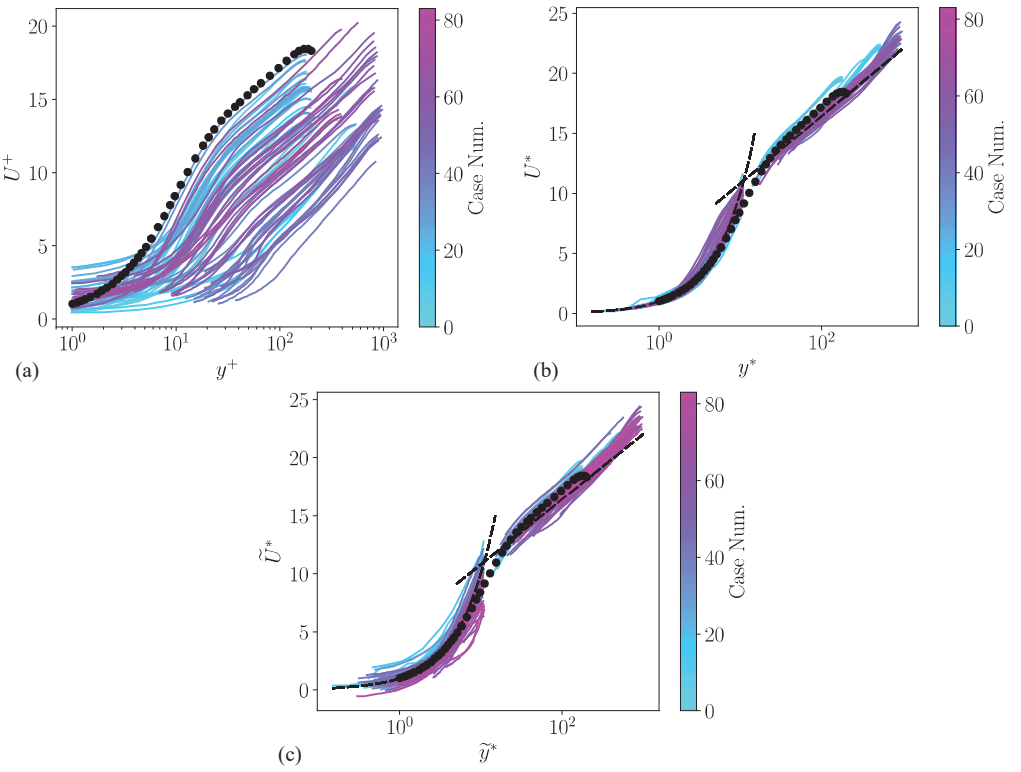

FIGURE 9. Velocity profiles for rough-wall boundary layers are presented in (a) as extracted DNS profiles, (b) as model form values obtained from DNS data for model fits and (c) as modeled data using Eqs. (4.3), (5.1), and (6.1). Additionally, we include an example smooth-channel DNS result from Thakkar *et al.* (2017) at $Re_\tau = 180$ (denoted by ●), along with the viscous sublayer profile ($U^+ = y^+$) and the log layer profile [$U^+ = (1/\kappa)\ln y^+ + B$] for reference.

considered geometries. This approach provides a practical and effective means to predict turbulent flows over a range of rough-wall surfaces.

Acknowledgements

This investigation was funded with the support of the Boeing Co., NASA's Transformational Tools and Technology (T3) Program, and the DoD SMART Fellowship.

REFERENCES

BUSSE, A., & JELLY, T. O. 2023 Effect of high skewness and kurtosis on turbulent channel flow over irregular rough walls. *J. Turbul.* **24**, 57–81.

CHAN, L., MACDONALD, M., CHUNG, D., HUTCHINS, N. & OOI, A. 2015 A systematic investigation of roughness height and wavelength in turbulent pipe flow in the transitionally rough regime. *J. Fluid Mech.* **771**, 743–777.

CHAN, L., MACDONALD, M., CHUNG, D., HUTCHINS, N. & OOI, A. 2018 Secondary motion in turbulent pipe flow with three-dimensional roughness. *J. Fluid Mech.* **854**, 5–33.

Chung, D., Hutchins, N., Schultz, M. P., & Flack, K. A. 2021 Predicting the drag of rough surfaces. *Annu. Rev. Fluid Mech.* **53**, 439–471.

Clauser, F. H. 1954 Turbulent boundary layers in adverse pressure gradients. *J. Aeronaut. Sci.* **21**, 91–108.

Colebrook, C. F., Blench, T., Chatley, H., Essex, E. H., Finniecome, J. F., Lacey, G., Williamson, J., & Macdonald, G. G 1939 Correspondence. turbulent flow in pipes, with particular reference to the transition region between the smooth and rough pipe laws.(includes plates). *J. Inst. Civ. Eng.* **12**, 393–422.

Colebrook, C. F. & White, C. M. 1937 Experiments with fluid friction in roughened pipes. *P. R. Soc. London* **161**, 367–381.

De Marchis, M., Saccone, D.m Milici, B. & Napoli, E. 2020 Large eddy simulations of rough turbulent channel flows bounded by irregular roughness: Advances toward a universal roughness correlation. *Flow Turbul. Combust.* **105** 2, 627–648.

Demirel, Y. K., Turan, O., & Incecik, A. 2017 Predicting the effect of biofouling on ship resistance using CFD. *Appl. Ocean Res.* **62**, 100–118.

Forooghi, P., Stroh, A., Magagnato, F., Jakirlić, S., & Frohnapfel, B. 2017 Toward a universal roughness correlation. *J. Fluids Eng.* **139**, 121–201.

Flack, K. A., & Chung, D. 2022 Important parameters for a predictive model of k_s for zero-pressure-gradient Flows. *AIAA J.* **60**, 5923–5931.

Flack, K. A., Schultz, M. P., & Barros, J. M. 2020 Skin friction measurements of systematically-varied roughness: Probing the role of roughness amplitude and skewness. *Flow Turbul. Combust.* **104**, 317–329.

Grigson, C. 1987 The full-scale viscous drag of actual ship surfaces and the effect of quality of roughness on predicted power. *J. Ship Res.* **31**, 189–206.

Hama, F. R. 1954 Boundary-layer characteristics for smooth and rough surfaces. *Trans. Soc. Nav. Arch. Marine Engrs.* **62**, 333–358.

Jimenez, J. 2004 Turbulent flows over rough walls. *Annu. Rev. Fluid Mech.* **36**, 173–196.

Jouybari, M. A., Yuan, J., Brereton, G. J., & Murillo, M. S. 2021 Data-driven prediction of the equivalent sand-grain height in rough-wall turbulent flows. *J. Fluid Mech.* **912**, A8.

Kadivar, M., Tormey, D., & McGranaghan, G. 2021 A review on turbulent flow over rough surfaces: Fundamentals and theories. *Int. J. Thermofluids* **10**, 100077.

Kuwata, Y. & Kawaguchi, Y. 2019 Direct numerical simulation of turbulence over systematically varied irregular rough surfaces. *J. Fluid Mech.* **862**, 781–815.

Ma, H., Li, Y., Yang, X., & Ye, L. 2023 Data-driven prediction of the equivalent sand-grain roughness. *Sci. Rep.* **13**, 19108.

Ma, R., Alamé, K., & Mahesh, K. 2021 Direct numerical simulation of turbulent channel flow over random rough surfaces. *J. Fluid Mech.* **908**, A40.

Napoli, E., Armenio, V., & de Marchis, M. 2008 The effect of the slope of irregularly distributed roughness elements on turbulent wall-bounded flows. *J. Fluid Mech.* **613**, 385–394.

Nikora, V., Goring, D., McEwan, I., & Griffiths, G. 2001 Spatially averaged open-channel flow over rough bed. *J. Hydraul. Eng.* **127**, 123–133.

Nikora, V., Koll, K., McEwan, I., McLean, S., & Dittrich, A. 2004 Velocity distribution in the roughness layer of rough-bed flows. *J. Hydraul. Eng.* **130**, 1036–1042.

Nikuradse, J. 1932 Laws of flows in rough pipes. *VDI Forschungsheft 361. Trans. NACA Tech. Memo. No. 1292*.

Thakkar, M., Busse, A., & Sandham, N. 2017 Surface correlations of hydrodynamic drag for transitional rough engineering surfaces. *J. Turbul.* **18**, 138–169.

Thakkar, M., Busse, A., & Sandham, N. 2018 Direct numerical simulation of turbulent channel flow over a surrogate for Nikuradse-type roughness. *J. Fluid Mech.* **837**, R1.

Yang, J., Stroh, A., Lee, S., Bagheri, S., Frohnapfel, B., & Forooghi, P. 2023 Prediction of equivalent sand-grain size and identification of drag-relevant scales of roughness–a data driven approach. *J. Fluid Mech.* **975**, A34.